

Flow visualisation to identify mechanisms leading to axis-switching of slotted synthetic jets

C. Fischer, R.N. Sharma and G.D. Mallinson

Department of Mechanical Engineering
University of Auckland, Auckland 1142, New Zealand

Abstract

Characteristics of a synthetic jet generated from a rectangular slot orifice of aspect ratio 35 have been investigated using Computational Fluid Dynamics simulations and flow visualisation techniques involving high speed camera photography. Some insight into the phenomenon of axis-switching is gained. In particular, it is revealed that the flows near the slot ends during expulsion and ingestion phases of each cycle lead to a vortex structure being formed that has a greater propagation velocity near the centre of the slot than at the ends, which aids axis switching. Further studies are underway to understand the mechanisms involved fully.

Introduction

In the last decade there has been a surge of research interest in developing flow controlling devices that can provide appreciable aerodynamic performance gain, do not require a large energy input from the operating device, and are cheap and lightweight at the same time.

One particular device that has received considerable attention is the synthetic jet actuator (SJA). A SJA consists of a vibrating membrane which oscillates and alternately sucks ambient air in and forces air out through a small orifice creating a jet. Indeed, this is the major benefit of the synthetic jet (SJ) compared to an ordinary continuous jet (CJ) which needs a constant, external fluid supply to maintain the jet. Consequently, the SJA has advantages of low cost but also simple structure and easy installation for which it has attracted much research over the last decade. The SJ has established itself as a useful fluidic device with increasing potential for practical applications, ranging from heat transfer enhancement and thrust vectoring of jet engines, to active control of flow separation and turbulence in boundary layers. This makes the SJA especially attractive for applications where energy consumption reduction is of much interest.

A number of studies have focused on the development of SJs. In spite of this, there is at present a limited availability of information regarding the fundamental understanding of vortex formation and its dependence on orifice geometry. The aim of this research is to investigate the slot SJ flow field by utilising CFD and flow visualisation techniques.

Synthetic Jets

A SJ can be created from ambient fluid and a moving wall (e.g. a diaphragm or membrane) usually at the bottom of a cavity opposite to the orifice operating in an oscillatory cycle. During the suction phase the fluid is entrained through the orifice into the cavity due to negative pressure inside the cavity created by the 'downward' moving membrane. Afterwards, the membrane moves 'upwards' and the jet is formed at the end of the discharge phase when the flow separates at the edge of the orifice. Depending on the initial conditions a vortical structure is formed which rolls up and subsequently moves away from the orifice

under its self-induced velocity. Depending on the shape of the orifice this vortical structure is round or ring-like. In detail, a vortical structure is formed as long as the pressure drop across the orifice is large enough to impart an impulse to the structure to overcome the influence of the orifice image and the flow forces during the suction phase [1]. It is noteworthy to mention that since the jet is developed from the ambient fluid the net mass flux over each cycle is zero.

The SJ can be laminar and transform to turbulent depending on the flow conditions. For 'minimum' formation criteria a laminar jet is created which changes to a transitional jet and finally a turbulent jet [2] as initial parameters are changed.

The main difference between a SJ and a CJ is the spread rate of the SJ which is always higher when similar flow properties are compared (e.g. equivalent Re). Similar to the CJ, the jet width increases and the centreline velocity decreases somewhere downstream where vortex breakdown takes place. Furthermore, the streamwise velocity for SJs decays much faster compared to an equivalent continuous jet [2].

Vortex Formation and Parameter

To ensure jet formation with vortex ring generation, the vortex ring forming at the orifice needs to have the ability to overcome the suction velocity during the ingestion stroke. In other words, the vortex ring needs to have a high enough self induced velocity or rather a high enough vortex strength to overcome this suction velocity. The vortex strength can be measured by the level of the relative vorticity Ω . If the circulation is large enough, i.e. the vorticity is strong enough, the vortex will roll-up at the orifice exit.

As soon as a vortex ring is formed at the orifice exit it starts to entrain external fluid. The increase in mass leads to a decrease in velocity and thus, the vortex ring grows in size but also slows down as it moves away from the orifice exit. As the vortex ring slows further down vorticity is transferred into the trailing wake and the ring eventually breaks down. Due to the alternating reversal in flow direction along the centreline a stagnation point is formed which influences vortex breakdown. At the beginning of the suction phase the strain rates are high at the stagnation point which leads to instabilities within the vortices, breakdown of these structures and thus the onset of small-scale transition [3, 1]. The transition process proceeds toward the rear end of the vortices, progresses through the fluid behind it and thereby sustains the jet.

For the jet formation in quiescent air it has been shown [3] that two independent dimensionless parameters characterise the flow of the SJ. The first parameter is the jet Reynolds number Re_d .

$$Re_d = U_{ave} d_o / \nu \quad (1)$$

which is based on the average orifice exit velocity U_{ave} during one cycle and the orifice diameter d_o or slot width w , and ν is the

kinematic viscosity of the fluid. The second parameter is the dimensionless stroke length L :

$$L = \frac{l}{d_o}, \quad (2)$$

where l is the stroke length:

$$l = \int_0^{T/2} U_{ave}(t) dt. \quad (3)$$

Re_d and L are used to estimate jet formation. For example, it was found that the threshold for round SJ formation in quiescent air occurs at $L=0.5$ [4]. Furthermore, Glezer and Amitay [1] have shown that there is no axisymmetric vortex ring formation for $L < 0.4$. Furthermore, a Strouhal number St can also be defined as:

$$St = \frac{f d_o}{U_{ave}}, \quad (4)$$

where f is the vortex shedding frequency.

The most recent work on jet formation criteria in quiescent air is that of Zhou et al. [5]. The findings in this study proved that a combination of a minimum St and a minimum L is necessary to ensure jet formation and jet formation with vortex roll-up. PIV and numerical simulations were used to verify the findings. It was shown that Ω is related to St as well as L and d_o/St_l (the orifice diameter to Stokes layer thickness ratio, which is defined as the radial distance between the peak velocity and the wall at the orifice exit [5]). In other words, a higher St and thus a thinner Stokes layer promotes vortex roll-up as long as L is high enough. This is contributed to a shift of the location of the peak velocity which enhances the exit velocity and hence effects the concentration of vorticity which leads to the formation. Finally, it was concluded that $St > 8.5$ and $L > 4$ needs to be fulfilled to ensure jet formation with vortex roll-up.

Characteristics of Synthetic Jets

For a round orifice and very low Re a laminar jet is created which turns into a laminar jet with vortex ring roll up with increasing Re . At a certain Re level the laminar rings break down and the jet becomes transitional. At high Re the SJ is fully turbulent.

A jet created from a round orifice is axisymmetric but turns into a planar jet for high AR slot orifices [3]. Slot orifice jets develop a particular phenomena called axis-switching. Here the jet develops along the major orifice axis in the beginning and switches usually by 90 degrees downstream in a way that the jet develops further across the major axis. This has been reported for both CJs and SJs [6, 7] but needs further investigation. Compared to a round CJ, the round SJ has a similar cross-stream velocity with a larger spreading rate. The decay of the centreline velocity of the round SJ is also constant (x^{-1}) and the slot SJ also decays with $x^{-0.5}$ [7]. The CJ decay is higher compared to the decay of an equivalent SJ.

The time mean velocity across the SJ orifice exit is zero, unlike the CJ. This can also be seen in the different regions of CJs and SJs. Whereas there are three distinct flow regions for a turbulent rectangular CJ [6], there are four such regions for an equivalent SJ [7]. For the CJ, these are: an initial quasi-plane-jet region which includes the potential core region, a transition zone, and a quasi-axisymmetric zone in the far field [6]. A turbulent rectangular SJ has the same regions except an additional distinct region in the near field, before the quasi-plane-jet region, which is an initial developing region where vortical structures form and interact [7].

Another remarkable difference between equivalent CJs and SJs is the eddy viscosity which is higher for the SJs. The turbulent-viscosity (also eddy-viscosity) hypothesis assumes that the momentum transfer in turbulent flows is due to the eddies. Higher eddy viscosity in a flow can be seen as a more turbulent flow and thus enhanced mixing can be assumed.

For high AR slots the SJ is likely to behave as a two-dimensional planar jet in the near field. This is likely to change in the far field where the jet becomes three-dimensional [7].

Methodology

The commercial software package ANSYS CFX [8] is used for the numerical simulations; the model of the SJA is shown in Figure 1. The whole model consists of all parts which are used in the physical experiment, however, the loudspeaker at the bottom is modelled as a sinusoidal moving wall.

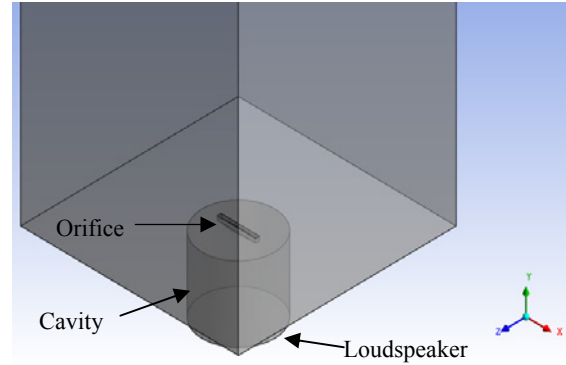


Figure 1: SJA model in CFX

A combination of the Shear Stress Transport (SST) and the Scale-Adaptive Simulation (SAS) turbulence model were used for the simulations. The SST model is a $k-\omega$ based turbulence model which switches between a $k-\omega$ model in the near wall region and a $k-\epsilon$ model in the free stream region. The model was developed to predict the onset and the amount of flow separation under adverse pressure gradients using the Gamma Theta transition model [9]. The SAS-SST model is a URANS equation formulation. The concept of the SAS utilises the von Kármán length-scale in the turbulence scale equation which allows Large Eddy Simulation (LES) like behaviour in unsteady regions and RANS behaviour in stable regions [10].

Flow field visualisations were assisted with the creation of the so called Q field or Q -criterion which is defined as the second invariant of the velocity gradient tensor D in CFX [11]:

$$D = \begin{bmatrix} \frac{\partial u}{\partial x} & \frac{\partial u}{\partial y} & \frac{\partial u}{\partial z} \\ \frac{\partial v}{\partial x} & \frac{\partial v}{\partial y} & \frac{\partial v}{\partial z} \\ \frac{\partial w}{\partial x} & \frac{\partial w}{\partial y} & \frac{\partial w}{\partial z} \end{bmatrix}. \quad (5)$$

Q is the combination of shear strain and vorticity and defined as:

$$Q = \left(\frac{\partial v}{\partial y} \cdot \frac{\partial w}{\partial z} - \frac{\partial v}{\partial z} \cdot \frac{\partial w}{\partial y} \right) + \left(\frac{\partial w}{\partial z} \cdot \frac{\partial u}{\partial x} - \frac{\partial w}{\partial x} \cdot \frac{\partial u}{\partial z} \right) + \left(\frac{\partial u}{\partial x} \cdot \frac{\partial v}{\partial y} - \frac{\partial u}{\partial y} \cdot \frac{\partial v}{\partial x} \right). \quad (6)$$

Creating isosurfaces for Q can help identifying vortex regions and flow structures. Figure 2 shows ring formations created from a circular orifice compared to smoke visualisation in the laboratory.

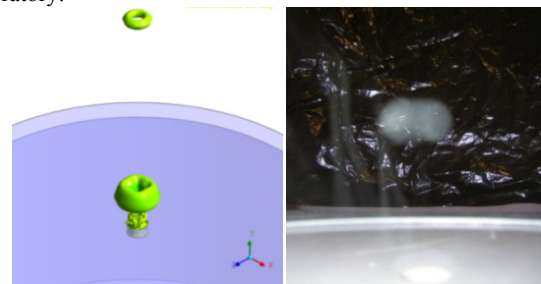


Figure 2: Vortex ring in simulation and physical experiment

The visual comparison shows good agreement to physical experiments. Nevertheless, the usage of the Q-criterion is still under debate as it is not a guarantee for the existence of vortical structures. Therefore, visualisations from experiments will be used to validate the computational results.

The actuator in the simulation is driven at a frequency of 60 Hz with an amplitude of 3 mm. The total computation time is 20 cycles with a solver convergence criterion of $RMS=5E-05$. The time step size is set to $T/500$ resulting in $3.33E-05$ sec per time step for this case. Three different meshes, listed below, are used to investigate the influence of the mesh. The SAS-SST turbulence and the Gamma-Theta transition model were used for all simulations.

Number of nodes	Computation time for 20 cycles on 4 CPUs
619 369	15 days
1 239 940	20 days
1 859 910	40 days

Table 1: Mesh size compared to computational effort

The relative error between the medium and the fine mesh has been found to be less than 2 % for velocity in the domain. Therefore, the medium mesh is used for further analysis. The additional computational effort outweighs the minor numerical accuracy benefits from using the fine mesh.

In the present investigations, $Re=4\ 450$ and $St=0.09$ were used which means that the SJ so generated will be in the laminar to the laminar ring regime.

The high speed camera Olympus i-speed 2 [12] was used to photograph the jets for comparison with simulation data. The minimum resolution of the camera is 60 fps and the maximum resolution is 33 000 fps. With increasing temporal resolution more light is needed and the picture resolution is decreased resulting in a minimum image size of 96x72 pixels.

Results and Discussion

Figures 3 - 5 show pictures from a high speed camera observation during one cycle of the actuation through a slot with an AR of 35. The jet initially develops spanwise i.e. along the slot but then appears to flip over (Figure 7) and continues developing across the slot. This is known as axis-switching.

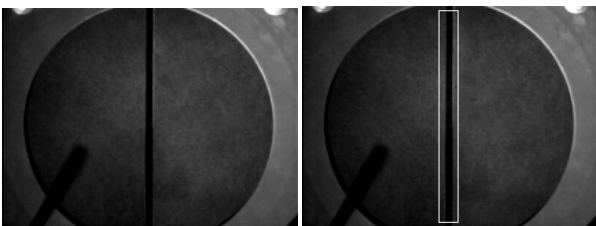


Figure 3: Begin of cycle (l) and expulsion (r)

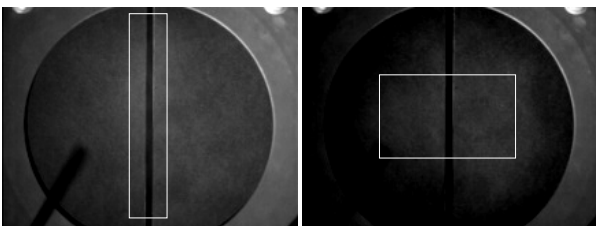


Figure 4: Jet along slot (l) and jet across slot (r)

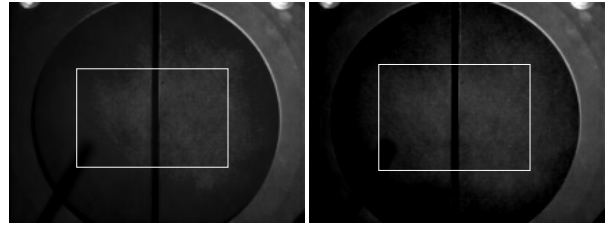


Figure 5: Jet widens (l) and end of cycle (r)

This behaviour shown in the smoke visualisation can be seen in present CFD simulations as well and is shown in Figures 6 - 8.

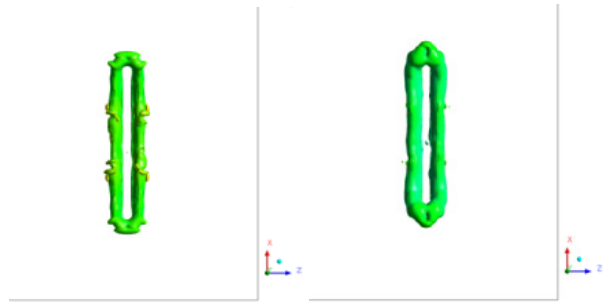


Figure 6: Begin of cycle (l) and expulsion (r)

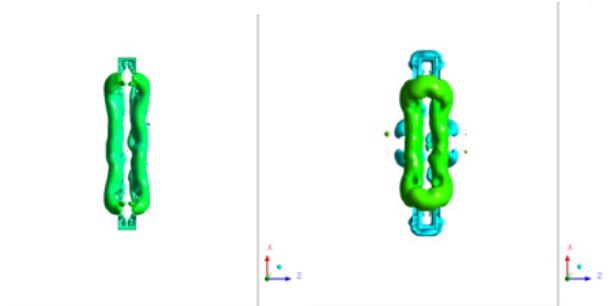


Figure 7: Jet along slot (l) and jet turns across slot (r)

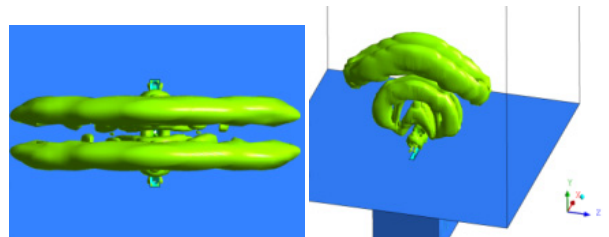


Figure 8: Jet widens across slot (l) and isometric view at end of several cycles (r)

An explanation for the axis-switching can be found by having a look at velocity vector plots in the major (along) and in the minor (across) slot axis during one cycle. Velocity vector plots (Figure 9) in the XY-plane (major axis) have shown the change in velocity around the orifice exit during one cycle. Initially, the fluid is entrained into the cavity. During this phase of the cycle the actuator is moving downwards. During the fluid expulsion phase as shown in the plots that follow, vortex formation is visible just at the orifice exit which rolls up at the orifice exit. The peak velocity is located near the ends of the slot but is shifting inwards while more ambient fluid is entrained by the vortical structure.

Following that, when the cycle repeats and the fluid is drawn back into the cavity, the entrainment is seen to be confined mostly around the ends of the slot while the fluid in the middle of the slot is at rest or still moving upwards. The vortical structure is moving inwards ‘pushing’ the fluid from the XY-plane into the YZ-plane (minor axis). Hence, the jet switches its axis. Other

velocity vector plots obtained from the YZ-plane (Figure 10) reveal that the vortex roll up starts later along the orifice compared to the roll up at the orifice ends. The fluid is accelerated at the ends earlier mainly because the fluid particles in the middle of the cavity are moving still downwards from the effects of the previous cycle. Particles in the middle in contrast are moving upwards, therefore enforcing the axis-switching.

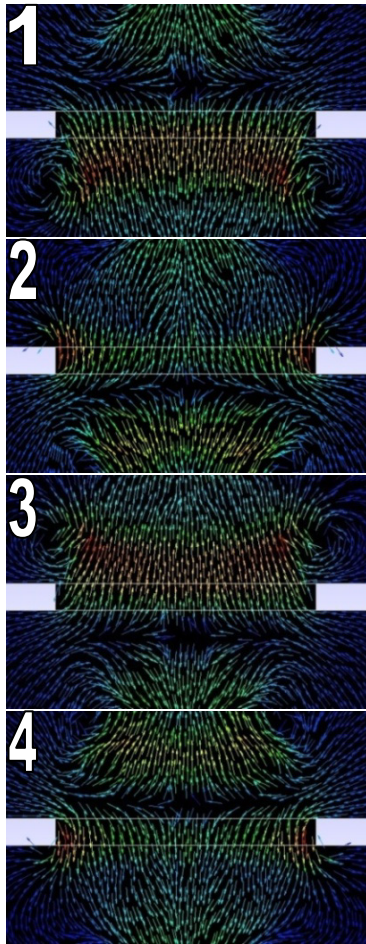


Figure 9: XY-plane at centre of SJA

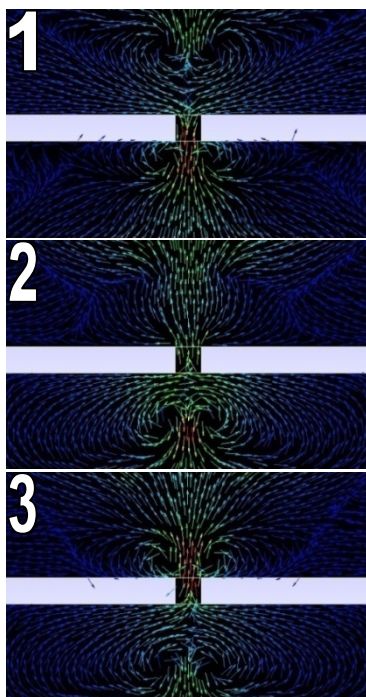


Figure 10: YZ-plane at centre of SJA

Conclusions

Smoke visualisation and CFD data have been compared and analysed in order to explain mechanisms leading to axis-switching in a slot synthetic jet. The high speed camera photography together with CFD has revealed that the phenomenon of axis-switching is related to the flow dynamics at the ends of the slot. In particular, during the suction phase, it has been established that fluid is entrained into the actuator cavity largely through the ends of the slot, causing a rapid dissipation of the roller vortices at the ends. This aids the vortices to assume an apparently transverse-wise orientation that one normally recognises as the phenomenon of axis-switching. Further studies are underway.

References

- [1] Glezer, A. and Amitay, M.: Synthetic jets. Annual Review of Fluid Mechanics, Vol. 34, 2002, pp. 503-529.
- [2] Cater, J. E. and Soria, J.: The evolution of round zero-net-mass-flux jets. Journal of Fluid Mechanics. 2002, Vol. 472, pp.167-200.
- [3] Smith, D. R., and Glezer, A.: The formation and evolution of synthetic jets. Physics of Fluid, Vol. 10, No. 9, 1998, pp. 2281-2297.
- [4] Jabbal, M., Wu, J. and Zhong, S.: The performance of round synthetic jets in quiescent flow. The Aeronautical Journal, Vol. 110, No. 1108, 2006, pp. 385-393.
- [5] Zhou, J., Tang, H. and Zhong, S.: Vortex roll-up criterion for synthetic jets. AIAA Journal, Vol. 47, No. 5, 2009, pp. 1252-1262.
- [6] Mi, J., Deo, R. C. And Nathan, G. J.: Characterisation of turbulent jets from high-aspect-ratio rectangular nozzles. Physics of Fluids. Vol. 17, 2005.
- [7] Krishnan, G. and Mohseni, K.: An experimental and analytical investigation of rectangular synthetic jets. Journal of Fluids Engineering. Vol. 131, 2009.
- [8] ANSYS CFX Introduction: Release 12.1. November 2009.
- [9] Langtry, R. B. and Menter, F. R.: Transition modeling for general CFD applications in aeronautics. AIAA, 2005-522.
- [10] ANSYS CFX-Solver Theory Guide: Release 12.1. November 2009.
- [11] ANSYS CFX-Post User's Guide: Release 12.1. November 2009, pp. 103-107.
- [12] Olympus. High Speed Video. i-SPEED 2. Features & Specifications. Issue 2: Printed KI UK 5049806/1009.